Published in final edited form as:
Bone. 2008 June ; 42(6): 1226–1234. doi:10.1016/j.bone.2008.02.007.

Bone Tissue Engineering with Premineralized Silk Scaffolds

Hyeon Joo Kim[1], **Ung-Jin Kim**[1,2], **Hyun Suk Kim**[1,3], **Chunmei Li**[1], **Masahisa Wada**[4], **Gary G. Leisk**[1], and **David L. Kaplan**[1,*]

1 *Departments of Biomedical Engineering, Chemical & Biological Engineering; Mechanical Engineering and Bioengineering & Biotechnology Center, Tufts University, Medford, MA 02155, USA*

2 *Mecellose R&D Team, R&D Center, Samsung Fine Chemicals Co., Ltd., 103-1 Munji-dong, Yusung-gu, Taejeon 305-380, Korea*

3 *Department of Polymer Science and Engineering, Inha University, Incheon 402-751, Korea*

4 *Department of Biomaterials Science, Graduate School of Agricultural and Life Sciences, The University of Tokyo, Yayoi 1-1-1, Bunkyo-ku, Tokyo 113-8657, Japan*

Abstract

Silks fibroin biomaterials are being explored as novel protein-based systems for cell and tissue culture. In the present study, biomimetic growth of calcium phosphate on porous silk fibroin polymeric scaffolds was explored to generate organic/inorganic composites as scaffolds for bone tissue engineering. Aqueous-derived silk fibroin scaffolds were prepared with the addition of polyaspartic acid during processing, followed by the controlled deposition of calcium phosphate by exposure to $CaCl_2$ and Na_2HPO_4. These mineralized protein-composite scaffolds were subsequently seeded with human bone marrow stem cells (hMSC) and cultured *in vitro* for 6 weeks under osteogenic conditions with or without BMP-2. The extent of osteoconductivity was assessed by cell numbers, alkaline phosphatase and calcium deposition, along with immunohistochemistry for bone related outcomes. The results suggest increased osteoconductive outcomes with an increase in initial content of apatite and BMP-2 in the silk fibroin porous scaffolds. The premineralization of these highly porous silk fibroin protein scaffolds provided enhanced outcomes for the bone tissue engineering.

Keywords

osteogenesis; silk scaffold; hydroxyapatite; tissue engineering; stem cells

Introduction

Bones provide mechanical protection for internal organs and blood forming marrow, facilitate locomotion and serve as a reservoir for calcium, magnesium and phosphate minerals [1]. Bones are formed by a series of complex events involving mineralization with calcium phosphate in the form of hydroxyapatite (HAP) on extracellular matrix proteins primarily consisting of collagen type I. Calcium-phosphate (Ca-P) coatings have also been used to improve the

Correspondence should be address to: David Kaplan, Department of Biomedical Engineering, 4 Colby Street, Medford, Massachusetts 02155, USA, phone: 617-627-3251, fax: 617-627-3231, E-mail: E-mail: david.kaplan@tufts.edu.

bonding of polymeric materials to bone and to enhance cell adhesion and differentiation of osteoprogenitor cells [2,3]. Ca-P biomaterials are used as grafts for bone repair, augmentation, or substitution. These commercially-available Ca-P biomaterials differ in origin, composition, physical form and physicochemical properties, while offering similar compositions to bone mineral phases, bioactivity, promotion of cellular functions and osteoconductivity [4].

Bone fractures and related damage result in more than 1.3 million surgical procedures each year in the United States [5]. Many acute and chronic injuries or defects require bone graft substitutes. Current options include autografts, allografts, and an assortment of synthetic or biomimetic materials and devices. Each of these options has significant limitations, such as the need for second site of surgery, limited supply, inadequate size and shape, and the morbidity associated with donor site. Thus there remains a need for new options [4]. Tissue engineering has potential to address this need through the combination of biomaterials, growth factors, and cells. Highly porous scaffolds are generally used as the substrate for anchorage dependent cells and to facilitate nutrient and metabolite distribution to guide cell growth leading to new bone tissue formation [6]. For bone tissue engineering, biodegradable synthetic polymers such as poly (glycolic acid) (PGA), poly(lactic acid) (PLA), copolymers of poly(DL-lactic-glycolic acid) (PLGA), and biodegradable naturally derived polymers such collagen and fibrin have been studied in this context [7–10]. Salt-leaching methods are often used to generate the porous foams from these biodegradable polymers [11–14]. One of the limitations of the above approach is that new tissue matrix formation is often limited to the surface of the foams, with minimum cell growth near the center or necrotic zones in the center of the construct [6,7].

The goals for scaffolds for bone tissue engineering include appropriate chemistry, morphology and structure to promote cell adhesion for osteoblasts and osteoprogenitor cells, migration, differentiation, and synthesis of new bone matrix, with homogenous distribution to avoid necrosis in the central regions where transport is more limited [6]. Silk fibroin represents an important biomaterial in this context. While silk has a long history of use in sutures, recent studies have expanded the fundamental understanding of the formation and function of silk-based biomaterials. Silk fibroin materials offer impressive mechanical properties, biodegradability, biocompatibility, and versatility in processing for biomedical applications [15–21]. Previously, we have reported the formation of three-dimensional porous silk fibroin scaffolds prepared in an all-aqueous format [13,14] as well as an organic solvent-based (hexafluoroisopropanol; HFIP) process [22]. The porosity, pore size, and mechanical properties could be controlled by manipulation of the concentration of silk fibroin protein used in the process and the size of porogen (NaCl particles) [12,13,22]. Most importantly within the context of the limitations noted above with other degradable porous biodegradable scaffolds, silks degrade very slowly, they are stabilized without a need for chemical cross-linking, and thus these systems retain their open porous features longer to promote more homogenous growth of cells and new tissue formation [23–25].

HAP has been investigated for bone replacement since this material mimics natural bone mineral features [26–29]. HAP has been studied extensively in cell culture and possesses osteoconductivity [30–33]. We hypothesized that the incorporation of bone-like mineral HAP into highly porous biodegradable silk fibroin scaffolds would improve osteogenic outcomes. Therefore, in the present study, highly porous mineralized aqueous-derived silk fibroin scaffolds were prepared and mineralized with HAP. The effect of mineralization on osteogenic differentiation of hMSCs was assessed with respect to bone tissue engineering.

Materials and Methods

Materials

Fetal bovine serum (FBS), Minimum essential medium (MEM) αmedium, basic fibroblast growth factor (bFGF), Penicillin-streptomycin (Pen-Strep), Fungizone, non essential amino acids, and trypsin were from Gibco (Carlsbad, CA). Ascorbic acid phosphate, Histopaque-1077, dexamethasone, and β-glycerophosphate were from Sigma (St. Louis, MO). BMP-2 was a generous gift from Wyeth Bio-Pharmaceuticals (Andover, MA). All other substances were of analytical or pharmaceutical grade and obtained from Sigma. Silkworm cocoons were kindly supplied by M. Tsukada (Institute of Sericulture, Tsukuba, Japan).

Preparation of silk fibroin aqueous solution

Cocoons of *B. mori* were boiled for 20 min in an aqueous solution of 0.02 M Na_2CO_3, and then rinsed thoroughly with distilled water to extract the glue-like sericin proteins. The extracted silk fibroin was dissolved in 9.3 M LiBr solution at 60°C for 4 hrs, yielding a 20 w/v% solution. This solution was dialyzed in distilled water using a Slide-a-Lyzer dialysis cassette (MWCO 3,500, Pierce) for 2 days. The final concentration of silk fibroin aqueous solution was *ca.* 8 w/v%, which was determined by weighing the remaining solid after drying. To prepare concentrated silk fibroin solution, 10 ml of 8 w/v % silk fibroin solution was dialyzed against 1 liter of 25 wt% polyethylene glycol (PEG, 10,000 g/mol) solution at room temperature by using Slide-a-Lyzer dialysis cassettes (MWCO 3500) [13]. After the required time, the concentrated silk fibroin solution was slowly collected by syringe to avoid excessive shearing and the concentration was determined. All solutions were stored in a refrigerator at 7–8°C before use to avoid premature precipitation. Silk fibroin films prepared from 8 w/v % solutions were evaluated to verify the removal of Li^+ ion by XPS (X-ray photoelectron spectrometer, PHI 5600 ESCA microscope, Physical Electronics, Eden Prairie, MN, USA); no residual Li^+ ion was detected.

Preparation of silk fibroin-polyaspartic acid scaffolds

For the preparation of the polymer solutions the required amount of polyaspartic acid solution (20 wt%) was added to silk fibroin solution (8.0 ~ 9.8 wt%) with mild stirring for 2 minutes. The blend ratios of silk fibroin/polyaspartic acid were 100/0, 95/5, 90/10 and 80/20 (w/w). Aqueous-derived silk fibroin scaffolds were prepared by adding 4 g of granular NaCl (particle size; 850~1000 μm) into 2 ml of silk fibroin-polyaspartic acid solutions in disk-shaped containers with 18 mm in diameter and 20 mm in height. The containers were covered and left at room temperature. After 24 hrs, the containers were immersed in water and the NaCl extracted for 2 days.

Mineralization

The alternate soaking process was used to grow apatite on silk fibers. First, silk fibroin-polyaspartic acid scaffolds (5 mm in diameter × 5 mm in height) were soaked in 20 ml of 200 mM $CaCl_2$ solution (buffered with 50 mM Tris·HCl, pH 7.4) for 20 min at 37°C and washed two times with 200 ml of distilled water. The silk fibroin-polyaspartic acid scaffolds were then transferred to 20 ml of 120 mM Na_2HPO_4 solution, soaked for 20 min at 37°C and washed two times with times with 200 ml of distilled water. After soaking cycles were repeated 3, 5 and 7 times, mineralized scaffolds were freeze-dried.

Scanning Electron Microscopy (SEM)

Freeze-dried silk scaffolds were fractured in liquid nitrogen using a razor blade. Samples were sputter coated with gold. The morphology of the scaffolds was observed with a LEO Gemini 982 Field Emission Gun SEM. Pore size was obtained using *ImageJ* software developed at the

US National Institutes of Health. Four independent samples were conducted with a minimum of N=5 for pore size.

X-ray Photoelectron Spectroscopy (XPS)

XPS was performed using a Surface Science Inc. Model SSX-100 X-ray photoelectron spectrometer (PHI 5600 ESCA microscope, Physical Electronics, Eden Prairie, MN, USA). Survey scans and narrow scans (spot 1000 μm, resolution 4) were performed using a flood gun (charge neutralizer) setting of 5 eV to prevent charging of the sample surface.

X-ray diffraction

X-ray diffraction of freeze-dried samples of the scaffold was obtained with Ni-filtered Cu-Kα radiation (λ= 0.15418 nm) from a Rigaku RU-200BH rotating-anode X-ray generator operating at 40 kV and 40 mA. X-ray diffraction patterns were recorded with a point collimated beam and an imaging plate (Fuji Film BAS-IP SR 127) in an evacuated camera. The camera length was calibrated with NaF (d=0.23166nm).

Human Bone Marrow Stem Cell Isolation and Expansion

Total bone marrow (25 cm^3, Clonetics, Santa Rosa, CA) was diluted in 100 ml of medium (10% FBS) and prepared as we have previously reported [14]. Briefly, cells were separated by density gradient centrifugation with 20 ml aliquots of bone marrow suspension overlaid onto a poly-sucrose gradient (1,077 g/cm^3, Histopaque, Sigma, St. Louis, MO) and centrifuged at 800×g for 30 min at room temperature. Cells were pelleted and suspended in expansion medium (α-MEM, 10% FBS, 1 ng/ml bFGF, 100 U/ml penicillin, 100 μg/ml streptomycin, 0.25 μg/ml fungizone, 0.1 mM nonessential amino acids) and seeded in 75 cm^2 flasks at a density of 5×10^4 cells/cm^2. The adherent cells were allowed to reach approximately 80% confluence (12–17 days for the first passage). Cells were trypsinized, replated and passage 2 (P2) cells (80% confluence after 6–8 days), were used for the experiments.

In vitro Culture

For examination of cell growth and differentiation in vitro on the silk scaffolds, P2 hMSCs (5×10^6 cells/scaffold) were seeded onto prewetted (α-MEM, overnight) scaffolds (diameter ×height; 5 mm ×5 mm). After 24h, the medium was removed and cultures were maintained in individual wells of 6-well plates. Osteogenic media consisted of α-MEM supplemented with 10% FBS, 0.1 mM nonessential amino acids, 50 μg/ml ascorbic acid-2-phosphate, 100 nM dexamethasone, 10 mM β-glycerolphosphate and 100 ng/ml BMP-2 in the presence of 100 U/ml penicillin, 100 μg/ml streptomycin, and 0.25 μg/ml fungizone. Cultures were maintained at 37□ in a humidified incubator supplemented with 5% CO_2. Half of the medium was changed every 2–3 days. The scaffolds were cultured for 6 weeks and samples removed for analysis.

Biochemical Analysis

Scaffolds were processed for biochemical analysis and histology. Cell proliferation on the scaffolds was quantified with DNA assay. For DNA analysis, 4 scaffolds per group were chopped with microscissors in ice. DNA content (N=4) was measured using the PicoGreen assay (Molecular Probes, Eugene, OR), according to the protocol of the manufacturer. Samples were measured fluorometrically at an excitation wavelength of 480 nm and an emission wavelength of 528 nm. For total calcium content, samples (N=4) were extracted twice with 0.5 ml 5% trichloroacetic acid. Calcium content was determined by a colorimetric assay using o-cresolphthalein complexone (Sigma, St. Louis, MO). The calcium complex was measured spectrophotometrically at 575 nm. Alkaline phosphatase (ALPase) activity was measured using a biochemical assay from Sigma (St. Louis), based on conversion of p-nitrophenyl phosphate to p-nitrophenol, which was measured spectrophotometrically at 405 nm.

Histological evaluation

After fixation with 4% phosphate-buffered formaldehyde for at least 24 hours, specimens were embedded within paraffin and sectioned (5 μm). Using standard histochemical techniques, serial sections were stained with hematoxylin and eosin. Mineralization was analyzed using the von Kossa stain method.

Immunohistochemistry

Samples are fixed in 10% neutral buffered formalin for 8–12 hrs, dehydrated in graded alcohols, embedded in paraffin, and sectioned to a thickness of 5 μm. Sections are assessed immunohistochemically using the DAB Detection Kit (Ventana Medical Systems, Inc., Tucson, AZ) according to the manufacturer's instructions. Briefly, sections are digested with endopeptidese to unmask antigen binding sites, exposed to an endogenous peroxidase inhibitor, and incubated with primary col I antibody (Biodesign, Saco, ME) at room temperature. Sections are then incubated with biotinylated IgG and exposed to horseradish peroxidase (HRP) labeled streptavidin. Antibody complexes were visualized after the addition of a buffered diaminobenzidine (DAB) solution. The sections then were counterstained in hematoxylin and lithium carbonate and mounted. Negative controls are performed similarly in the absence of the primary antibody.

Mechanical properties

Mechanical characterization of compression properties of the scaffolds was performed on an Instron 3366 testing frame equipped with a 0.1 kN load cell. Compression tests were conducted at room temperature with a conventional open-sided (non-confined) configuration. A displacement control mode was used, with a crosshead displacement rate of 5 mm/min. Eleven cylindrical samples, each nominally 5 mm in diameter and 5 mm in height, were evaluated for each composition. This 1:1 sample geometry aspect ratio represents an acceptable compromise between processing and testing needs. The compressive stress and strain were graphed and the average compressive strength as well as the compressive modulus and standard deviation determined. The elastic modulus was calculated based on a semi-automatic technique. The stress-strain diagram from initial loading until just beyond initial failure of the samples (encompassing the linear, load-bearing portion of the diagram) was segmented into 8 sections. Least-squares' fitting was used to determine the slopes of each section. The steepest slope, which for all samples corresponded to the initial section of the load-bearing material response, was defined as the compressive modulus. The compressive strength was determined using an offset-yield approach. A line was drawn parallel to the modulus line, but offset by 0.5% of the sample gauge length (nominal sample height of 5 mm). The corresponding stress value at which the offset line crossed the stress-strain curve was defined as the compressive strength of the scaffold [13].

Statistical Analysis

Two independent experiments were conducted with a minimum of N=4 for each data point. The results (Fig. 3B, 4 and 6) of one independent experiment are displayed for each analysis. Data were analyzed using the Student-Newman-Keuls Multiple Comparisons Test.

Results

Preparation of aqueous-derived scaffolds

Porous silk fibroin (SF)-polyaspartic acid (PA) scaffolds were prepared using a salt-leaching method as we have previously described [13,34]; the salt leaching approach has also been reported for collagen and polylactic acid [11–14]. In the process used here the surface of the NaCl particles dissolve in the SF-PA aqueous solution, while most of the salt was retained in

the solid state because of super saturation of the solution. The SF-PA aqueous solutions formed into hydrogels after 24 hrs, resulting in the formation of water-stable porous matrices (Fig. 1). Subsequent to porous scaffold formation and removal of the residual salt, controlled deposition of apatite was carried out by salt deposition due to the nucleating role of the polyaspartic acid that partitions to the interface of the hydrophobic silk structures [34]. The amount of apatite in the scaffolds increased with increase in polyaspartic acid content and mineralization cycles used to control mineral phase deposition (Table 1). Apatite particles deposited on the scaffold walls with full coverage attained after three rounds of mineralization. The carboxyl groups from the polyaspartic acid enhanced apatite deposition on the silk fibroin substrates.

Morphology

Fig. 2A contains SEM images of the scaffolds prepared from blends of SF-PA solutions with NaCl particles (850~1000 μm). The actual pore sizes in the scaffolds were 750±20 μm, reflecting the partial dissolution of the surface of NaCl particles. The pore size distribution was homogeneous throughout the scaffolds. The scaffold pores were highly interconnected and displayed rough surfaces likely due to the partial dissolution on the surfaces of the NaCl particles resulting in a templating effect on the final surface morphology. The mineralized silk fibroin-polyaspartic acid scaffolds with various levels of mineralization are shown in Fig. 2B. Apatite particles formed on the surfaces in the presence of polyaspartic acid with more than three mineralization cycles were used in the study. Globule-like structures of apatite were observed on the pore wall surfaces, the sizes of which increased with increased numbers of mineralization cycles.

Structural analysis

Structural changes in the SF-PA scaffolds were determined by X-ray diffraction (Fig. 3A). Silk scaffolds without treatment with polyaspartic acid or mineralization showed peaks at 8.8°, 20.4° and 24.6°, corresponding to the β-sheet crystalline structure (silk II) of native silk fibroin [35]. These results indicate β-crystalline spacing of 9.9, 4.3 and 3.6 Å according to the 8.5°, 20.4° and 24.6° reflections, respectively. X-ray diffraction analysis of the silk fibroin scaffolds with polyaspartic acid and mineralization showed characteristic peaks of HAP at 25.9° and 32.0°. These peak intensities increased with increased numbers of mineralization cycles and polyaspartic acid content.

Mineralized matrix deposition

To determine the mineralized matrix deposition in the aqueous-derived silk scaffolds, a calcium assay was used. As the number of mineralization cycles and polyaspartic acid content increased, calcium deposition increased. The exception was the calcium deposition in the silk scaffolds with 10% polyaspartic acid, which was higher than those with 20% polyaspartic acid (Fig. 3B). To confirm that calcium measurements represent active mineralization, the scaffolds without mineralization were assayed under identical same condition and no calcium was detected.

Mechanical properties

Compression testing revealed similar stress-strain behavior for all samples: an initially shallow (low modulus) linear region, followed by a short stress plateau representing scaffold yielding, before a final region of increased loading as the samples were completely flattened. This ductile, sponge-like behavior was observed for all mineralized aqueous-derived silk scaffold samples as well as the aqueous-derived silk scaffolds. Modulus and compressive strength were lower in the SF-PA samples ($p<0.01$, Fig. 4) in comparison to the nonmineralized samples. Like a multi-story building with soft walls, the porous scaffolds likely fail in a progressive-collapse manner. As compression load is increased, some scaffold walls begin to deform and

collapse. The overall integrity of the scaffold may not be compromised by this localized event. However, as load increases, an increasing number of walls will fail, leading to scaffold collapse. This material response can be seen in stress-strain diagrams as low-amplitude load oscillations. In this context, while apatite particles may have been deposited on scaffold walls in localized regions, there may not be sufficient coverage to provide global stiffening.

Scanning electron microscope evaluation after cell culture

Four groups of mineralized scaffolds were prepared for *in vitro* cultivation. The blend ratios of SF/PA (w/w) were 100/0 (group I), 95/5 (group II), 90/10 (group III) and 80/20 (group IV) with five rounds of mineralization, based on the results above regarding polyaspartic acid content and cycles to complete surface coverage. hMSCs were seeded on all four groups of mineralized silk 3-D scaffolds and maintained with or without BMP-2 in osteogenic medium for 6 weeks. After 6 weeks most pores were filled with new tissue mass as observed by SEM. The constructs cultured with or without BMP-2 contained connective tissues and mineralized nodules throughout the constructs (Fig. 5).

Biochemical evaluation

The DNA content of the hMSC-scaffolds was measured to quantify cell proliferation. After 6 weeks of growth the cell numbers on scaffolds of group IV (20% polyaspartic acid) were slightly higher than those on the other mineralized scaffolds. Cell proliferation was not affected by BMP-2 throughout the constructs (Fig. 6A). Alkaline phosphatase (ALPase) activity, a marker of early osteoblastic differentiation and commitment of hMSCs toward the osteoblastic phenotype [36], was determined after 6 weeks of culture. For scaffolds without BMP-2, ALPase activity increased by 36% on constructs of group IV when compared with the level found in the constructs of group I ($p < 0.01$). From group IV, the ALPase activity of cell/mineralized silk constructs cultured in osteogenic media with BMP-2 was higher ($p<0.001$) than the activity in constructs cultured in osteogenic media without BMP-2 (Fig. 6B). Calcium content was determined after 6 weeks in culture. With BMP-2 (100 ng/ml) present in culture mineralized matrix deposition on the scaffolds was higher ($p<0.001$) than scaffolds cultured without BMP-2. Increased content of polyaspartic acid resulted in a progressive increase in mineralized matrix deposition (Fig. 6C). Without BMP-2 in the cultures, similar levels of calcium deposition on the scaffolds were observed.

Histological and immunohistochemical evaluation

Cell distribution and morphologies were visualized by histological analysis using hematoxylin and eosin (Fig. 7A). As the polyaspartiac acid content increased cells were less uniformly distributed without BMP-2 in culture. Cells were uniformly distributed in control scaffolds (without mineralization, data not shown). On all mineralized aqueous-based silk scaffolds the cells were more abundant on the surface regions than in the center regions 6 weeks after cell seeding. However hMSCs were more uniformly distributed in scaffolds of group I than in group IV. Osteoblast-like cells with cuboidal or columnar morphologies were observed in all mineralized aqueous-based silk scaffolds. After 6 weeks of culture, most pores were filled with connective tissue, fibroblast-like cells and cuboidal osteoblast-like cells. The pores were filled with extracellular matrix (ECM). Von Kossa staining supported calcification on the surface of scaffold lattices, with prominence for scaffolds of group IV in comparison to scaffolds of group I. In scaffolds of group I, mineralization was also observed in the internal lattice. After 6 weeks, mineralization was advanced on all mineralized aqueous-based silk scaffolds in the presence of BMP-2 (Fig. 7B). Immunohistochemistry analysis demonstrated that collagen type I (Col I) was expressed in all groups. With BMP-2 in culture, Col 1 expression slightly increased in constructs of group II and III (Fig. 7C).

Discussion

From the primary sequence of the silkworm silk fibroin heavy chain, large internal hydrophobic blocks and small internal hydrophilic blocks are present, with two large hydrophilic blocks at the chain ends [37]. The percentage of hydrophobic residues in silk fibroin is 79% [38] and the repetitive sequence in these hydrophobic blocks consists of GAGAGS peptides that dominate the β-sheet structure that forms the crystalline regions in silk fibroin fibers and films [39]. Since protein solubility typically decreases as salt concentration rises, interactions between these domains become favored from both intra- and interchain interactions. Interactions between non-polar residues increase with addition of salt, leading to the salting-out effect [40]. The behavior of the fibroin in the concentrated NaCl system may be related to the role of the salt ions in extracting water that would otherwise coat the hydrophobic fibroin domains, promoting chain-chain interactions leading to the new more stable structure. These changes in hydrophobic hydration induce protein folding, resulting in β-sheet formation [41]. We have previously shown that these macroporous 3D aqueous-based silk scaffolds improved bone-related outcomes for bone tissue engineering [13,14].

The development of a new generation of bone-like composite materials with improved mechanical properties and enhanced biocompatibility requires a biomimetic synthetic approach using natural bone as a guide. The preparation of a range of bone-like materials has been reported [6,29,42–49]. Natural bone is a biocomposite in which inorganic apatite crystals are deposited on collagen fibers woven into a three dimensional structure. HAP-binding proteins have definitive HAP-binding sites based on acid side chains on amino acids. Proteins containing aspartic acid-rich sequences interact with crystals of calcium salt in a specific manner [50,51], and poly-glutamic acid sequences or poly-aspartic acid sequences are present in HAP-binding proteins [49]. From a comparison of Fig. 3,5 and 6, and Table 1, as the poly-aspartic concentration was increased, the deposition of HAP increased. HAP consists of Ca^{2+} ions surrounded by both PO_4^{2-} and OH^- ions. Once the apatite nuclei form, spontaneous growth occurs by addition of calcium and phosphate ions from the surrounding medium during soaking in $CaCl_2$ and Na_2HPO_4 to trigger the deposition of apatite [49,52].

In the present study, a material similar in composition and structure to natural bone was hypothesized to be a good starting point for bone tissue engineering. Based on our prior studies with silk fibroin porous scaffolds without premineralization, we presumed suitable bone tissue outcomes would be found. The mineralization was anticipated to provide an enhanced environment for bone related outcomes due to the osteoconductivity, as well as improved mechanical properties. For the *in vitro* study of the 3D mineralized silk scaffolds, BMP-2 was added to the culture medium as it is known to induce osteogenic differentiation of hMSCs. Examination of cell-seeded constructs by SEM provided visual confirmation of good mineralization. Pores of the constructs were filled by cells at 6 weeks. More than a single cell layer was observed. Cells showed no regular orientation and mineralized nodules were formed in the constructs (Fig. 5). Proliferation, ALPase activity, and mineralization were assessed to monitor the behavior of hMSCs cells for osteogenic differentiation. Cells proliferated with time in the scaffolds in culture, demonstrating that the scaffold architecture was suitable for hMSC seeding and growth. Alkaline phosphatase levels were used as a marker since it is one of the markers of osteogenic cells [36,53,54], and osteoblast-like cells possess calcium receptors [55]. The bone matrix consists of hydroxyapatite crystals containing calcium and phosphorus. Therefore, these factors provide important indicators of osteogenic differentiation.

In the absence of BMP-2, ALPase activity and calcium deposition were similar in the mineralized silk scaffold groups. Also, similar ALPase activity was observed after 6 weeks in culture with osteogenic media, with or without BMP-2, in scaffolds of groups I, II and III. ALPase activity increased in scaffolds of group IV with BMP-2. Calcium measurements

revealed an increase in calcium deposition in all mineralized silk scaffolds with BMP-2 (Fig. 6B and 6C). Control scaffolds (without mineralization) showed no detectable calcium deposition after 6 weeks (data not shown). On von Kossa staining as the apatite mineral deposition on scaffold walls increased, osteoconductivity improved and (Fig. 7B).

The seeded hMSCs were more uniformly distributed in the scaffolds of control and group I compared with the other groups. As the polyaspartic acid content was increased the apatite mineral deposition increased and cells were less uniformly distributed in the scaffolds. The increase of apatite mineral particles may impede cell migration and permeability for nutrients to the center of scaffolds (Fig. 7A), as has often been observed in other porous scaffold systems as mentioned earlier. The adsorption of proteins and other biologically active molecules to HAP is likely different than to the control silk fibroin polymers without the mineral phase. These proteins and biologically active molecules may mediate the interactions between the cells and the scaffolds. The varied interactions from the scaffolds to the cells might have resulted in some of the change in osteoconductivity of the scaffolds [6].

In conclusion, aqueous-derived porous silk fibroin scaffolds could be used as templates to deposit apatite on the pore surfaces via mixing with polyaspartic acid during processing, followed by mineralization with $CaCl_2$ and Na_2HPO_4. The content of polyaspartic acid and the extent of mineralization impacted cell responses, with some of the conditions resulting in enhanced outcomes related to bone tissue engineering.

Acknowledgments

The authors thank the NIH P41 Tissue Engineering Resource Center for support of this program.

References

1. Boskey, AL. Mineralization, structure, and function of bone. In: Seibel, M.; Robins, S.; Bilezikian, J., editors. Dynamics of bone and cartilage metabolism. San Diego, CA: Academic press; 1999. p. p153-64.
2. Vehof JWM, Dolder J, Ruijter E, Spauwen PHM, Jansen JA. Bone formation in CaP-coated and noncoated titanium fiber mesh. J Biomed Mater Res 2003;64A:417–26.
3. Salgado AJ, Figueiredo JE, Coutinho OP, Reis RL. Biological response to pre-mineralized starch based scaffolds for bone tissue engineering. J Mater Sci Mater Med 2005;16:267–75. [PubMed: 15744619]
4. LeGeros RZ. Properties of osteoconductive biomaterials: calcium phosphates. Clin Orthop Relat Res 2002;395:81–98. [PubMed: 11937868]
5. Langer R, Vacanti J. Tissue engineering. Science 1993;260:920–6. [PubMed: 8493529]
6. Ma PX, Zhang R, Xiao G, Franceschi R. Engineering new bone tissue in vitro on highly porous poly (α-hydroxy acids)/hydroxyapatite composite scaffolds. J Biomed Mater Res 2001;54:284–93. [PubMed: 11093189]
7. Sikavitsas VI, Bancroft GN, Mikos AG. Formation of three-dimensional cell/polymer constructs for bone tissue engineering in a spinner flask and a rotating wall vessel bioreactor. J Biomed Mater Res 2002;62:136–48. [PubMed: 12124795]
8. Ochi K, Chen G, Ushida T, Gojo S, Segawa K, Tai H, Ueno K, Ohkawa H, Mori T, Yamaguchi A, Toyama Y, Hat J-I, Umezawa A. Use of isolated mature osteoblasts in abundance acts as desired-shaped bone regeneration in combination with a modified poly-DL-lactic –co-glycolic acid (PLGA)-collagen sponge. J Cell Physiol 2003;194:45–53. [PubMed: 12447988]
9. Yamada Y, Boo JS, Ozawa R, Nagasaka T, Okazaki Y, Hata K, Ueda M. Bone regeneration following injection of mesenchymal stem cells and fibrin glue with a biodegradable scaffold. J Cranio-maxillofac Surg 2003;31:27–33.
10. Rocha LB, Goissis G, Rossi MA. Biocompatibility of anionic collagen matrix as scaffold for bone healing. Biomaterials 2002;23:449–56. [PubMed: 11761165]

11. Ma, PX.; Langer, R. Fabrication of biodegradable polymer foams for cell transplantation and tissue engineering. In: Morgan, J.; Yarmush, M., editors. Tissue engineering methods and protocols. Totowa, NJ: Humana Press; 1999. p. 47-56.
12. Maquet V, Blacher S, Pirard R, Pirard JP, Jérôme R. Characterization of Porous Polylactide Foams by Image Analysis and Impedance Spectroscopy. Langmuir 2000;16:10463–70.
13. Kim UJ, Park J, Kim HJ, Wada M, Kaplan DL. Three-dimensional aqueous-derived biomaterial scaffolds from silk fibroin. Biomaterials 2005;26:2775–85. [PubMed: 15585282]
14. Kim HJ, Kim UJ, Vunjak-Novakovic G, Min B-H, Kaplan DL. Influence of Macroporous Protein Scaffolds on Bone Tissue Engineering from Bone Marrow Stem Cells. Biomaterials 2005;26:4442–52. [PubMed: 15701373]
15. Sofia S, McCarthy MB, Gronowicz G, Kaplan DL. Functionalized silk-based biomaterials for bone formation. J Biomed Mater Res 2001;54:139–48. [PubMed: 11077413]
16. Altman GH, Diaz F, Jakuba C, Calabro T, Horan RL, Chen J, Lu H, Richmond J, Kaplan DL. Silk-based biomaterials. Biomaterials 2003;24:401–16. [PubMed: 12423595]
17. Lee, KY.; Kong, SJ.; Park, WH.; Ha, WS.; Kwon, IC. J Biomater Sci Polym. Vol. 9. 1998. Effect of surface properties on the antithrombo-genicity of silk fibroin/S-carboxymethyl kerateine blend films; p. 905-14.
18. Santin M, Motta A, Freddi G, Cannas M. In vitro evaluation of the inflammatory potential of the silk fibroin. J Biomed Mater Res 1999;46:382–9. [PubMed: 10397996]
19. Panilaitis B, Altman GH, Chen J, Jin HJ, Karageorgiou V, Kaplan DL. Macrophage responses to silk. Biomaterials 2003;24:3079–85. [PubMed: 12895580]
20. Lam KH, Nijenhuis AJ, Bartels H, Postema AR, Jonkman MF, Pennings AJ, Nieuwenhuis P. Reinforced poly (L-lactic acid) fibres as suture material. J Appl Biomater 1995;6:191–7. [PubMed: 7492810]
21. Rossitch E Jr, Bullard DE, Oakes WJ. Delayed foreign-body reaction to silk sutures in pediatric neurosurgical patients. Childs Nerv Syst 1987;3:375–8. [PubMed: 3329961]
22. Nazarov R, Jin HJ, Kaplan DL. Porous 3-D scaffolds from regenerated silk fibroin. Biomacromolecules 2004;5:718–26. [PubMed: 15132652]
23. Meinel L, Karageorgiou V, Hofmann S, Fajardo R, Snyder B, Li C, Zichner L, Langer R, Vunjak-Novakovi G, Kaplan DL. Engineering bone-like tissue *in vitro* using human bone marrow stem cells and silk scaffolds. J Biomed Mater Res 2004;71A:25–34.
24. Meinel L, Hofmann S, Karageorgiou V, Zichner L, Langer R, Kaplan DL, Vunjak-Novakovic G. Engineering cartilage-like tissue using human mesenchymal stem cells and silk protein scaffolds. Biotechnol Bioeng 2004;88:379–91. [PubMed: 15486944]
25. Wang Y, Kim U-J, Blasioli DJ, Kim HJ, Kaplan DL. In Vitro cartilage tissue engineering with 3D porous aqueous-derived silk scaffolds and mesenchymal stem cells. Biomaterials 2005;26:7082–94. [PubMed: 15985292]
26. Akao M, Aok H, Kato K. Mechanical properties of sintered hydroxyapatite for prosthetic applications. J Mater Sci 1981;16:809–12.
27. Driessen AA, Klein CP, de Groot K. Preparation and some properties of sintered beta-whitelockite. Biomaterials 1982;3:113–6. [PubMed: 7082737]
28. Best S, Bonefield W. Processing behaviour of hydroxyapatite powders with contrasting morphology. J Mater Sci: Mate Med 1994;5:516–21.
29. Zhang R, Ma PX. Poly(α-hydroxy acids)/hydroxyapatite porous composites for bone-tissue engineering. I. Preparation and morphology. J Biomed Mater Res 1999;44:446–55. [PubMed: 10397949]
30. Puleo DA, Holleran LA, Doremus RH, Bizios R. Osteoblast responses to orthopedic implant materials in vitro. J Biomed Mater Res 1991;125:711–23. [PubMed: 1874756]
31. Jansen JA, van der Waerden JP, Wolke JG. Histologic investigation of the biologic behavior of different hydroxyapatite plasma-sprayed coating in rabbits. J Biomed Mater Res 1993;27:603–10. [PubMed: 8314812]
32. Akao M, Sakatsume M, Aoki H, Takagi T, Sasaki S. In vitro mineralization in bovine tooth germ cell cultured with sintered hydroxyapatite. J Mater Sci: Mater Med 1993;4:569–74.

33. Klein CP, Patka P, Wolke JG, de Blieck-Hogervorst JM, de Groot K. Long-term in vivo study of plasma-sprayed coatings on titanium alloys of tetracalcium phosphate, hydroxyapatite and alpha-tricalcium phosphate. Biomaterials 1994;15:146–50. [PubMed: 8011861]
34. Li CM, Jin HJ, Botsaris GD, Kaplan DL. Silk apatite composites from electrospun fibers. J Mater Res 2005;20:3374–84.
35. Asakura T, Kuzuhara A, Tabeta R, Saito H. Conformation characterization of *Bombyx mori* silk fibroin in the solid state by high-frequency ^{13}C cross polarization-magic angle spinning NMR, X-ray diffraction, and infrared spectroscopy. Macromolecules 1985;18:1841–5.
36. Lian JB, Stein GS. The developmental stages of osteoblast growth and differentiation exhibit selective responses of genes to growth factors (TGF beta 1) and hormones (vitamin D and glucocorticoids). J Oral implantol 1993;19:95–105. [PubMed: 8246305]
37. Zhou CZ, Confalonieri F, Medina N, Zivanovic Y, Esnault C, Yang T, Jacquet M, Janin J, Duguet M, Perasso R, Li ZG. Fine organization of *Bombyx mori* fibroin heavy chain gene. Nucleic Acids Res 2000;28:2413–9. [PubMed: 10871375]
38. Braun FN, Viney C. Modelling self assembly of natural silk solutions. Int J Biol Macromol 2003;32:59–65. [PubMed: 12957301]
39. Mita K, Icimura S, James TC. Highly repetitive structure and its organization of the silk fibroin gene. J Mol Evol 1994;38:583–92. [PubMed: 7916056]
40. Robinson DR, Jencks WP. The effect of concentrated salt solutions on the activity coefficient of acetyltetraglycine ethyl ether. J Am Chem Soc 1965;87:2470–9. [PubMed: 14327155]
41. Li GY, Zhou P, Shao ZZ, Xie X, Chen X, Wang HH, Chunyu LJ, Yu TY. The natural silk spinning process. A nucleation-dependent aggregation mechanism? Eur J Biochem 2001;268:6600–6. [PubMed: 11737214]
42. Miyaji F, Kim H-M, Handa S, Kokubo T, Nakamura T. Bonelike apatite coating on organic polymers: novel nucleation process using sodium silicate solution. Biomaterials 1999;20:913–9. [PubMed: 10353645]
43. Ignjatovic N, Tomic S, Dakic M, Miljkovic M, Plavsic M, Uskokovic D. Synthesis and properties of hydroxyapatite/poly-L-lactide composite biomaterials. Biomaterials 1999;20:809–16. [PubMed: 10226707]
44. Bradt J-H, Mertig M, Teresiak A, Pompe W. Biomimetic mineralization of collagen by combined fibril assembly and calcium phosphate formation. Chem Mater 1999;11:2694–2701.
45. Bigi A, Boanini E, Panzavolta S, Roveri N. Biomimetic growth of hydroxyapatite on gelatin films doped with sodium polyacrylate. Biomacromolecules 2000;1:752–6. [PubMed: 11710207]
46. Hartgerink JD, Beniash E, Stupp SI. Self-assembly and mineralization of peptide-amphiphile nanofibers. Science 2001;294:1684–8. [PubMed: 11721046]
47. Song J, Saiz E, Bertozz CR. A new approach to moralization of biocompatible hydrogel scaffolds: An efficient process toward 3-dimensional bonelike composites. J Am Chem Soc 2003;125:1236–43. [PubMed: 12553825]
48. Goissis G, Maginador SVS, Martins VCA. Biomimetic mineralization of charged collagen matrices: in vitro and in vivo study. Artif Organs 2003;27:437–43. [PubMed: 12752204]
49. Yin YJ, Luo XY, Cui JF, Wang CY, Guo SM, Yao KD. A Study on biomineralization behavior of *N*-methylene phosphochitosan scaffolds. Macromol Biosci 2001;4:971–7. [PubMed: 15487022]
50. Fujisawa R, Wada Y, Nodasaka Y, Kuboki Y. Acidic amino acid-rich sequences as binding sites of osteonectin to hydroxyapatite crystals. Biochim Biophys Acta 1996;1292:53–60. [PubMed: 8547349]
51. Addadi L, Weiner S. Interactions between acidic proteins and crystals: Stereochemical requirements in biomineralization. Proc Natl Acad Sci USA 1985;82:4110–4. [PubMed: 3858868]
52. Gorski JP. Acidic phosphoproteins from bone-matrix-a structural rationalization of their role in biomineralization. Calcif Tissue Int 1992;50:391–6. [PubMed: 1596774]
53. Ciapetti G, Ambrosio L, Savarino L, Granchi D, Cenni E, Baldini N, Pagani S, Guizzardi S, Causa F, Giunti A. Osteoblast growth and function in porous poly ε-caprolactone matrices for bone repair: a preliminary study. Biomaterials 2003;24:3815–24. [PubMed: 12818554]
54. Henthorn, PS. Alkaline Phosphatase. In: Bilezikian, JP.; Raisz, LG.; Rodan, GA., editors. Principles of Bone Biology. San Diego, CA: Academic press; 1996. p. p197-206.

55. Leis HJ, Zach D, Huber E, Ziermann L, Gleispach H, Windischhofer W. Extracellular CA2+ sensing by the osteoblast-like cell-line, MC3T3-E1. Cell Calcium 1994;15:447–56. [PubMed: 8082128]

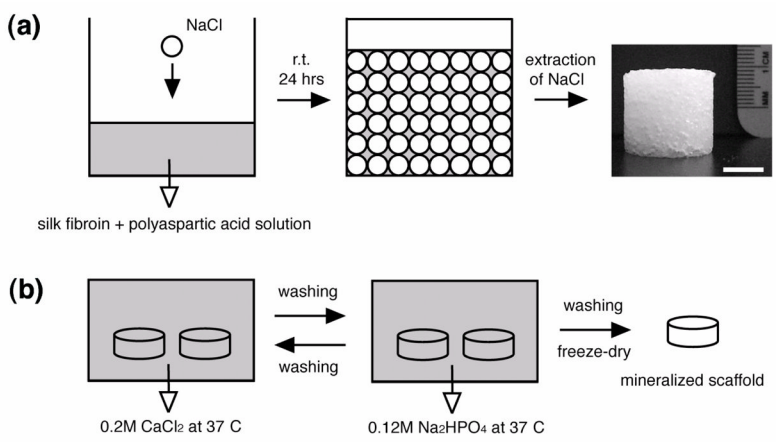

Fig. 1.

Schematic of the basic process (a) to prepare aqueous-derived 3D scaffolds from silk fibroin and polyaspartic acid, and (b) mineralization. Scale bar in 'a' = 1 cm.

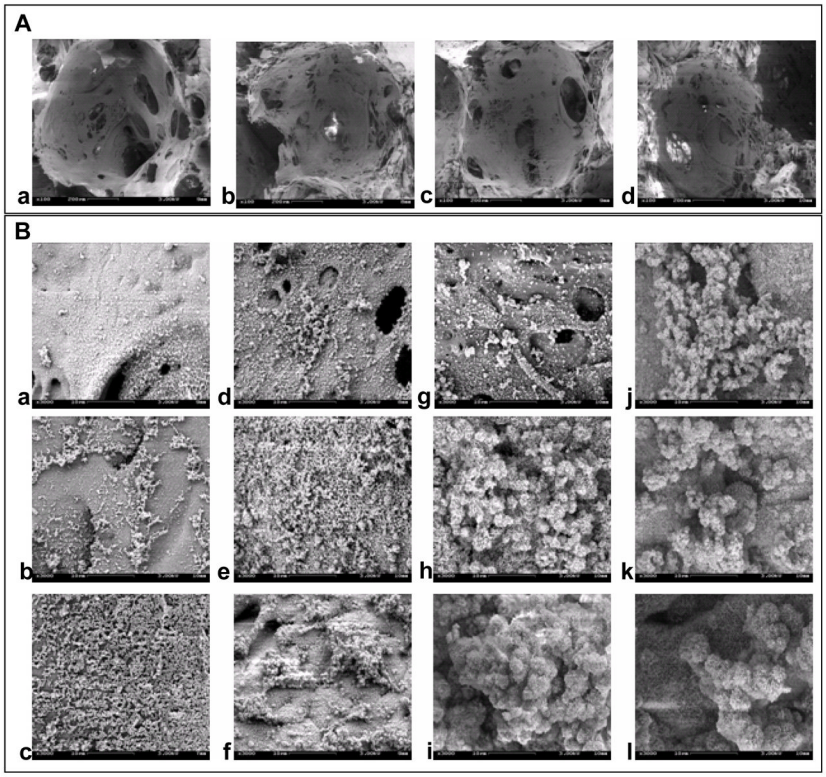

Fig. 2.

SEM images of the scaffolds prepared from various blend ratios of silk fibroin-polyaspartic acid solutions (A) [a; 100/0, b; 95/5, c; 90/10, d; 80/20]. Scale bar = 200 μm. SEM images of the mineralized scaffolds prepared from various blend ratios of silk fibroin-polyaspartic acid solutions (B) [100/0: a, b, c; 95/5: d, e, f; 90/10: g, h, I; 80/20: j, k, l] with various soaking cycles [3 cycles: top; 5 cycles: middle; 7 cycles: bottom]. Scale bar = 10 μm.

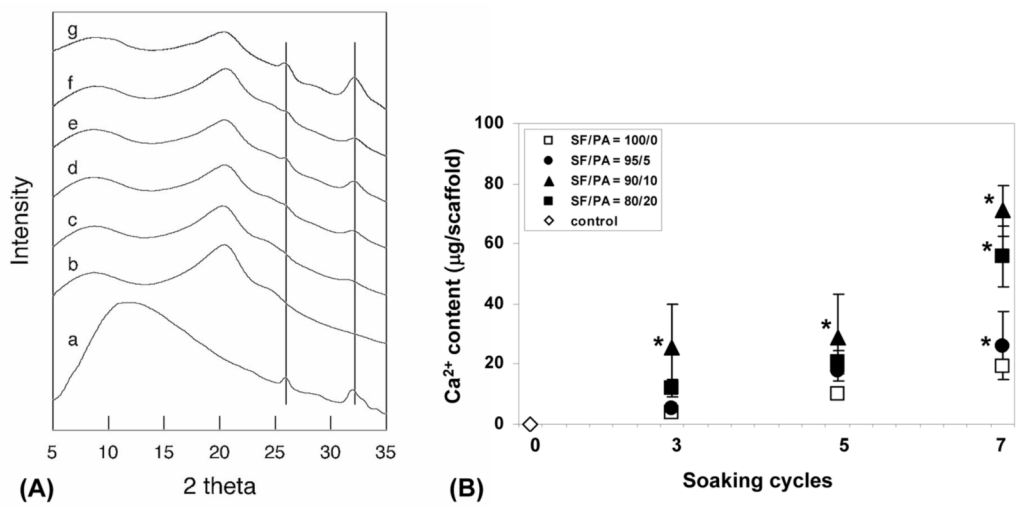

Fig. 3.

X-ray diffraction of silk fibroin scaffolds with and without the treatment of polyaspartic acid and mineralization (A). a; hydroxyapatite, b; silk fibroin (SF)/polyaspartic acid (PA) = 100/0 and 0 soaking cycle, c; SF/PA = 100/0 and 3 soaking cycles, d; SF/PA = 100/0 and 5 soaking cycles, e; SF/PA = 100/0 and 7 soaking cycles, f; SF/PA = 95/5 and 3 soaking cycles, g; SF/PA = 95/5 and 7 soaking cycles. Calcium deposition in silk fibroin scaffolds with and without the treatment of polyaspartic acid and mineralization (B). Silk fibroin scaffolds with or without the treatment of PA soaked in $CaCl_2$ and Na_2HPO_4 Tris buffer alternatively. Data are shown as mean ± standard deviation, from 4 samples. (*) represents statistically significant differences ($p<0.001$).

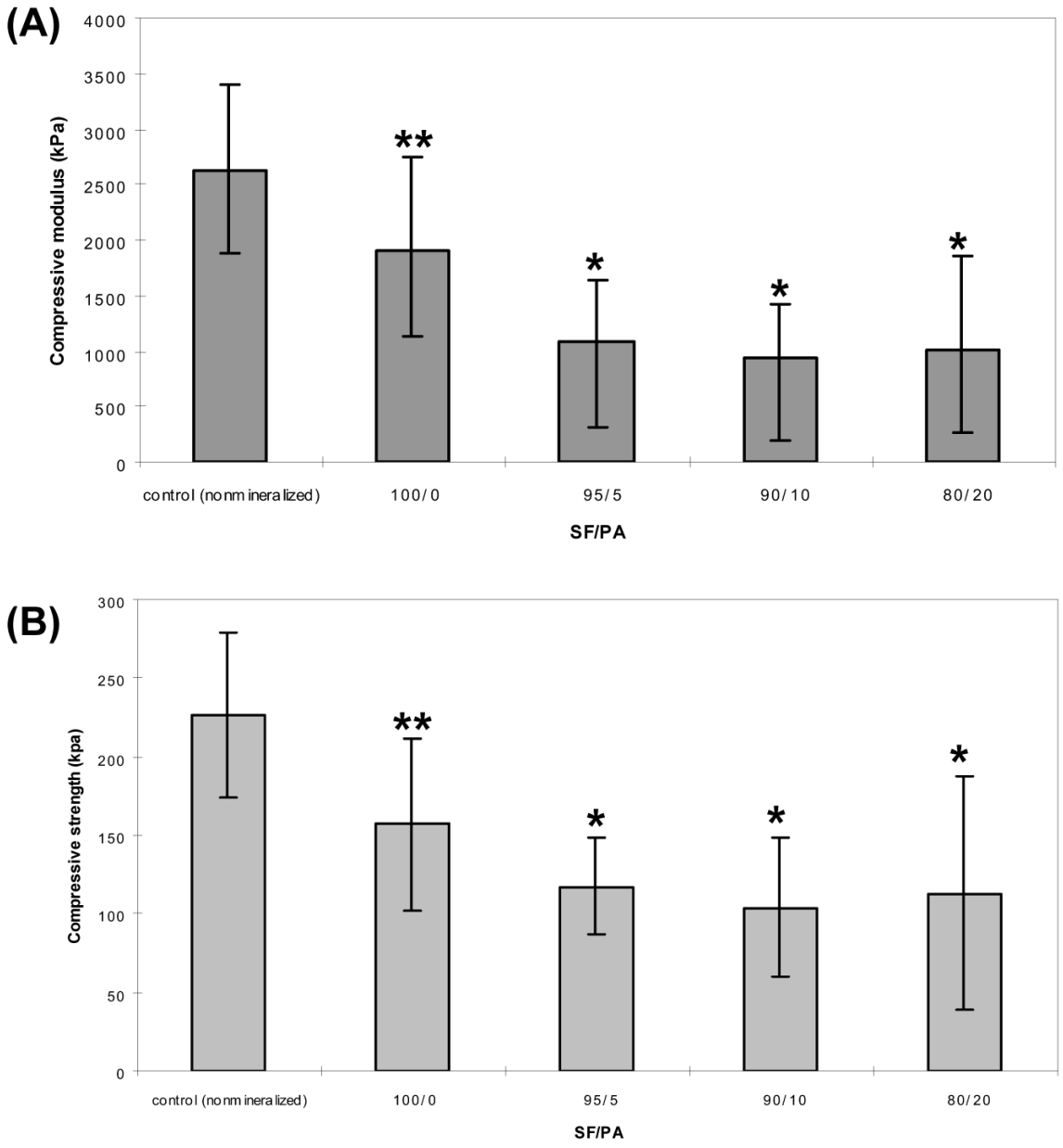

Fig. 4.

Compressive modulus (A) and strength (B) of aqueous-derived silk scaffolds and mineralized aqueous-derived silk scaffolds. (* and **) represents statistically significant differences ($p<0.001$ and $p<0.01$).

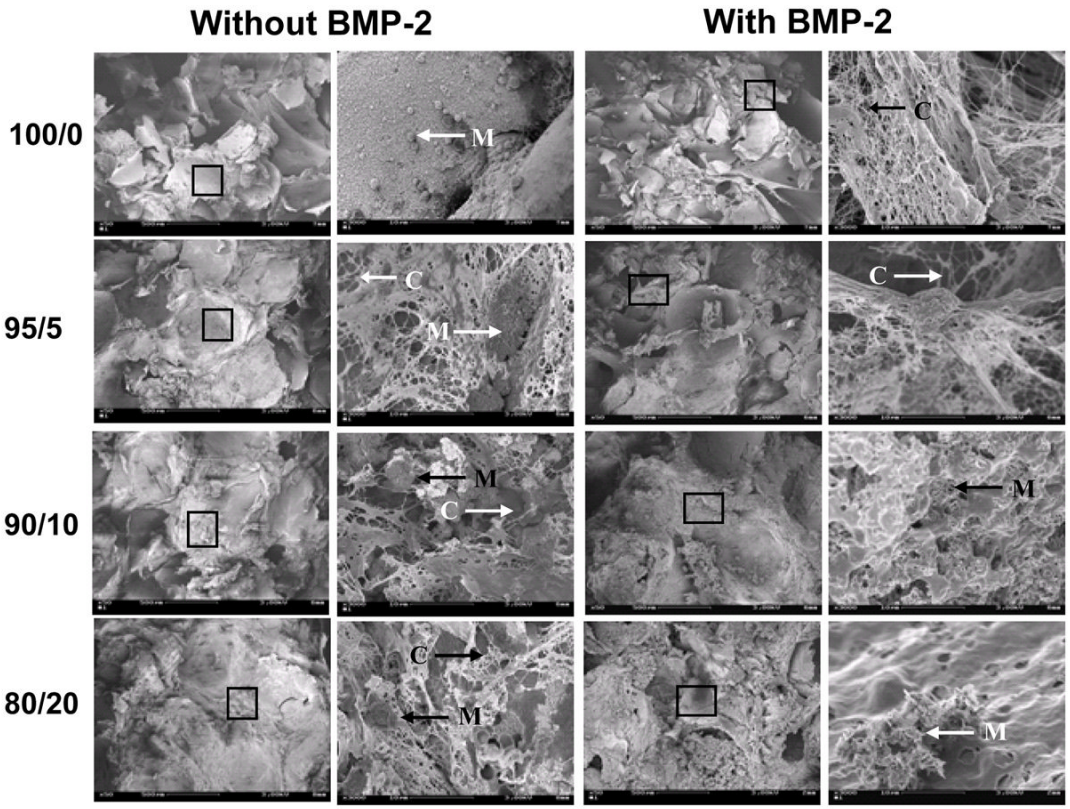

Fig. 5.

SEMs of cellular constructs maintained with osteogenic supplements. The constructs with hMSCs cultured for 6 weeks in osteogenic medium with BMP-2 (100 ng/ml) or without BMP-2. Connective tissues (C) and mineralized nodules (M) were formed in the constructs.

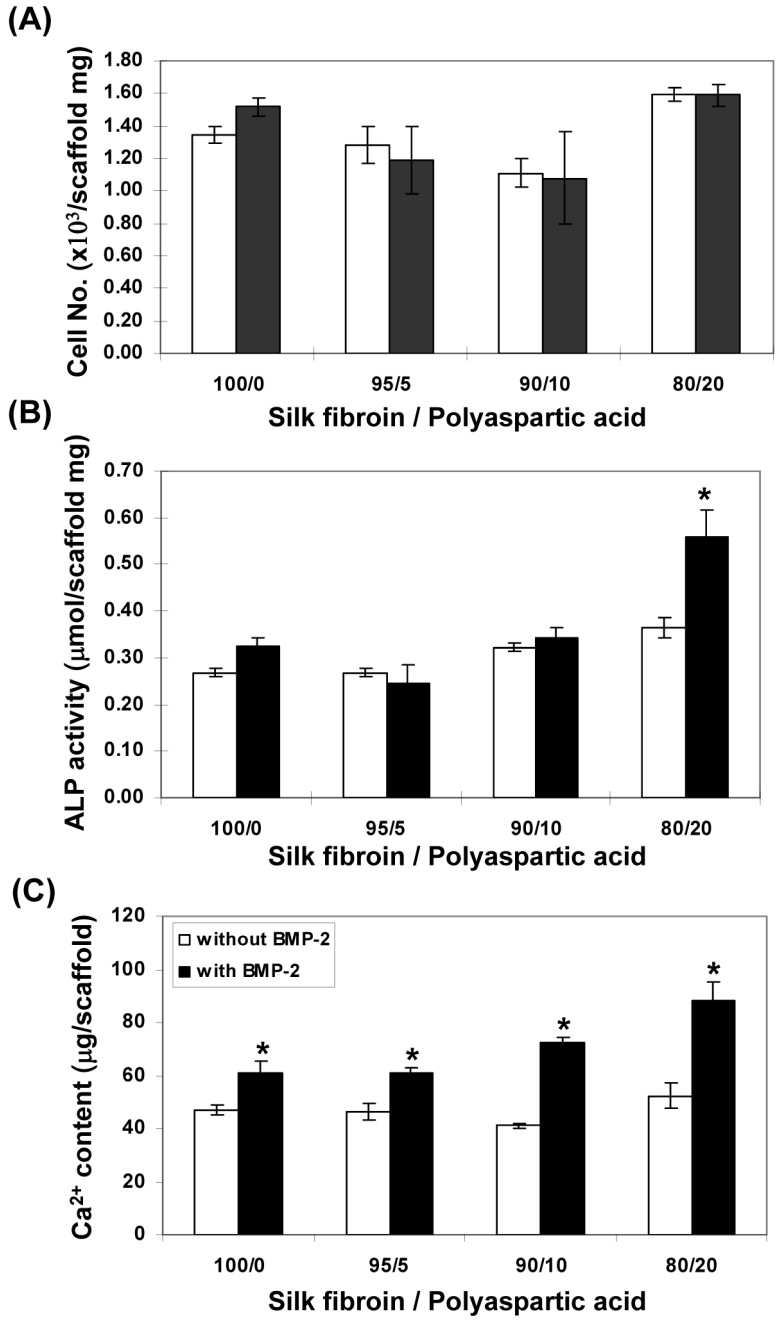

Fig. 6.

Biochemical characterization. Total number of cells on scaffolds after 6 weeks of culture (A). ALPase activity per-scaffold (B), total calcium per-scaffold (C). Data are shown as mean ± standard deviation, from 4 samples. (*) represents statistically significant differences ($p < 0.001$).

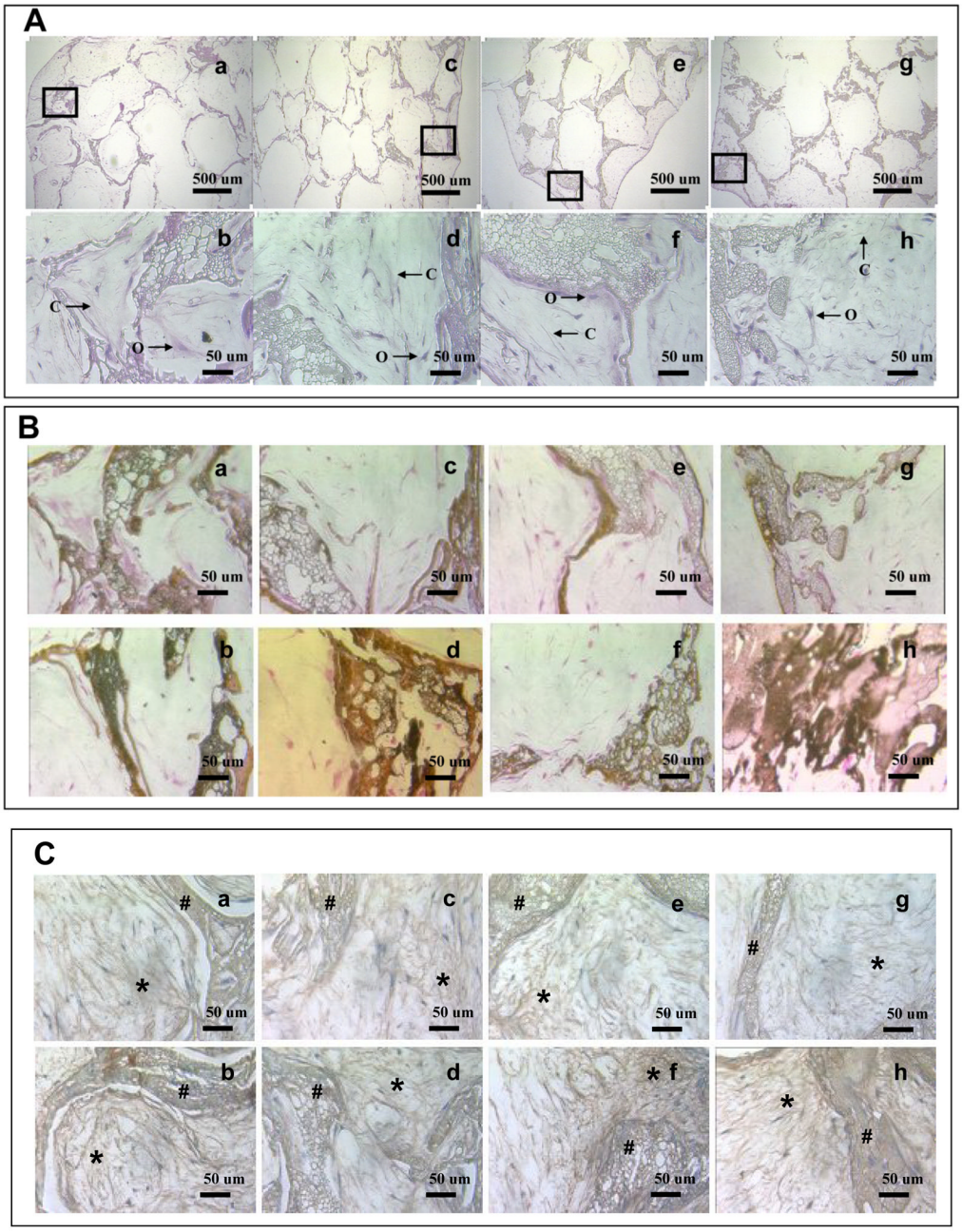

Fig. 7.

(A) Hematoxylin and eosin staining of cells on mineralized silk constructs. The constructs with hMSCs cultured for 6 weeks in osteogenic medium. Osteoblast-like cells (O) and connective tissues (C) were observed in the mineralized silk constructs. The scaffolds prepared from various blend ratios of silk fibroin-polyaspartic acid solutions (a, b: 100/0; c, d: 95/5; e, f: 90/10; g, h: 80/20) with 5 mineral deposition cycles. (B) Deposition of mineralized matrix on mineralized silk constructs. von Kossa staining (dark brown area) is shown for hMSCs cultured on mineralized silk constructs. The constructs with hMSCs cultured for 6 weeks in osteogenic medium with BMP-2 (100 ng/ml; b, d, f, h) or without BMP-2 (a, c, e, g). (C) Immunohistochemical staining of collagen type I. Extracellular matirices (*) stained positive for Col I within the scaffold pores. The Col I matrix covered the entire mineralized aqueous-

based silk lattice (#) after 6 weeks of culture with BMP-2 (100 ng/ml; b, d, f, h) or without BMP-2 (a, c, e, g).

Table 1

XPS results from the silk fibroin-polysaspartic acid (SF/PA) scaffolds

SF/PA	cycles	C_{1s}' %	N_{1s}, %	O_{1s}, %	Ca_{2p}, %	P_{2p}, %
100/0	0	61.4	16.0	21.4		
	3	50.7	12.3	29.0	4.8	3.2
	5	39.2	5.8	39.1	9.3	6.6
	7	31.1	4.5	44.5	11.4	8.6
95/5	0	61.1	17.1	21.6		
	3	34.9	5.8	40.9	10.9	7.5
	5	29.6	3.0	46.5	13.3	7.6
	7	26.5	1.5	47.1	14.3	10.5
90/10	0	61.0	17.5	21.6		
	3	31.4	5.4	43.0	10.9	9.3
	5	29.7	4.8	44.4	11.7	9.4
	7	23.6	2.8	48.1	13.6	11.3
80/20	0	60.4	17.9	21.7		
	3	33.3	4.6	42.4	11.7	8.0
	5	23.6	2.8	48.1	13.6	11.3
	7	22.0	1.5	49.5	14.6	12.1